FASTKIT: A Mobile Cable-Driven Parallel Robot for Logistics

Nicolò Pedemonte, Tahir Rasheed, David Marquez-Gamez, Philip Long, Étienne Hocquard, Francois Babin, Charlotte Fouché, Guy Caverot, Alexis Girin, Stéphane Caro

FASTKIT: A Mobile Cable-Driven Parallel Robot for Logistics

Nicolò Pedemonte, Tahir Rasheed, David Marquez-Gamez, Philip Long, Étienne Hocquard, Francois Babin, Charlotte Fouché, Guy Caverot, Alexis Girin, and Stéphane Caro

Abstract The subject of this paper is about the design, modeling, control and performance evaluation of a low cost and versatile robotic solution for logistics. The robot under study, named FASTKIT, is obtained from a combination of mobile robots and a Cable-Driven Parallel Robot (CDPR). FASTKIT addresses an industrial need for fast picking and kitting operations in existing storage facilities while being easy to install, keeping existing infrastructures and covering large areas. The FASTKIT prototype consists of two mobile bases that carry the exit points of the CDPR. The system can navigate autonomously to the area of interest. Once the desired position is attained, the system deploys the CDPR in such a way that its workspace corresponds to the current task specification. The system calculates the required mobile base position from the desired workspace and ensures the controllability of the platform during the deployment. Once the system is successfully deployed, the set of stabilizers are used to ensure the prototype structural stability. Then the prototype gripper is moved accurately by the CDPR at high velocity over a large area by controlling the cable tension.

N. Pedemonte, D. Marquez-Gamez, E. Hocquard, F. Babin, C. Fouché and A. Girin
IRT Jules Verne, Chemin du Chaffault, 44340, Bouguenais, France, e-mail: `{nicolo.`
`pedemonte,david.marquez-gamez,etienne.hocquard,francois.babin,`
`charlotte.fouche,alexis.girin}@irt-jules-verne.fr`

T. Rasheed
Centrale Nantes, Laboratoire des Sciences du Numérique de Nantes, UMR CNRS 6004, 1, rue de la Noë, 44321 Nantes, France, e-mail: `tahir.rasheed@ls2n.fr`

P. Long
RIVeR Lab, Department of electrical and computing engineering, Northeastern University, USA, e-mail: `p.long@northeastern.edu`

G. Caverot
B2A Technology, Mordelles, France, e-mail: `guy.caverot@basystemes.fr`

S. Caro
CNRS, Laboratoire des Sciences du Numérique de Nantes, UMR CNRS 6004, 1, rue de la Noë, 44321 Nantes, France, e-mail: `stephane.caro@ls2n.fr`

1 Introduction

Cable-Driven Parallel Robots (CDPRs) form a particular class of parallel robots whose moving platform is connected to a fixed base frame by cables. The cables may be coiled/uncoiled by motorized winches allowing a contro system to adjust the cable lengths between the winch exit points and the cable attachment points on the platform. Appropriate length adjustment of cables allows one to control the degrees of freedom of the moving platform. CDPRs have several advantages such as mechanical simplicity and a potentially very large workspace. They have been used in several applications, e.g. heavy payload handling and airplane painting [1], cargo handling [2], warehouse applications [3], large-scale assembly and handling operations [4], and fast pick-and-place operations [5]. Other possible applications include the broadcasting of sporting events, haptic devices Fortin2014, simulators [7], and search and rescue deployable platforms [8]. The performance improvement of CDPRs is still a challenge because the cable unilaterality (cables can pull but cannot push) makes their analysis much more complex than parallel robots with rigid legs. Indeed, it is necessary to introduce cable models in the analysis, that are usually complex, non-linear, non-algebraic and computer demanding.

As we have seen CDPRs may perform various kinds of applications but they impose a strong requirement regarding the free circulation of the cables without interference with the environment. It is therefore reasonable to adjust their geometry (which has a large influence on the performances) according to the task requirements and the robot's environment. FASTKIT has aimed therefore at developing an mobile, deployable and autonomous CDPRs, called Mobile Cable-Driven Parallel Robots (MCDPRs), that can be adapted to the logistic task. From a mechanical point of view changing the geometry of CDPR is relatively easy either by moving the winches, by using pulleys to modify the location of the winches exit points or by changing the location of the cable attachment points on the load. Preliminary studies on reconfigurable CDPRs were performed in the context of the NIST RoboCrane project [9]. Izard *et al.* [10] also studied a family of RCDPRs for industrial applications. Beside the mechanical modularity, a challenge is to develop a strategy that will allow one to determine the best CDPR geometry for a given task to be fulfilled. Discrete reconfigurations where the locations of the cable exit points are selected from a finite set of possible values have been recently studied in [11].

This paper deals with the design, modeling and performance analysis of a Mobile Cable-Driven Parallel Robot (MCDPR), named FASTKIT, developed in the framework of ECHORD++ FASTKIT project. FASTKIT project addresses an industrial need for fast picking and kitting operations in existing storage facilities while being easy to install, keeping existing infrastructures and covering large areas. Nowadays there exist several robotic solutions for logistic applications. One of the most popular automatic storage systems is the multi-shuttle system described in [11], which guarantees high performance in terms of working rate. The main drawbacks of such systems are the high investment cost, the long installation time and the lack of flexibility.

Fig. 1 FASTKIT concept: A cable-driven parallel robot mounted on two mobile platforms

Such systems are usually installed over large warehouses presenting a high entry and exit flow of storage boxes. In such conditions, an acceptable Return On Investment (ROI) is usually guaranteed. On the other hand, this solution is no longer possible or profitable for small warehouses, where there is no room for the installation of a large multi-shuttle system, or for warehouses characterized by a very low entry and exit flow of storage units, for which the high investment cost of a multi-shuttle solution is not justified.

The FASTKIT concept shown in Fig. 1 and developed in the scope of FASTKIT project is made up of CDPR mounted on two mobile platforms. As a result, it combines the autonomy of mobile robots with the advantages of CDPR, namely, large workspace, high payload-to-weight ratio, low end-effector inertia, deployability and reconfigurability. Moreover, CDPRs lead generally to low cost and easy maintenance solutions. Thanks to their characteristics, CDPRs can be used for different tasks such as the manipulation of heavy payloads or fast pick-and-place operations. Indeed, logistics is a very interesting field of application for CDPRs. Accordingly, FASTKIT aims at providing the user with a flexible and low cost logistic solution to equip small warehouses.

Therefore, the novelty of FASTKIT lies in the combination of autonomous mobile platforms and a CDPR. The main challenge in FASTKIT dealt with the design, modeling and assembly of the CDPR and the two mobile bases as well as the synchronization of their control laws.

This paper is organized as follows. Section 2 describes the main components, the control strategy and the architecture of the navigation stack of FASTKIT. Section 3 deals with to the kinematic modeling and kinematic performance evaluation of FASTKIT. The wrench capability of FASTKIT is assessed in Sec. 4. Some discussions and conclusions are given in Sec. 5.

2 FASTKIT Prototype

Fig. 2 FASTKIT prototype

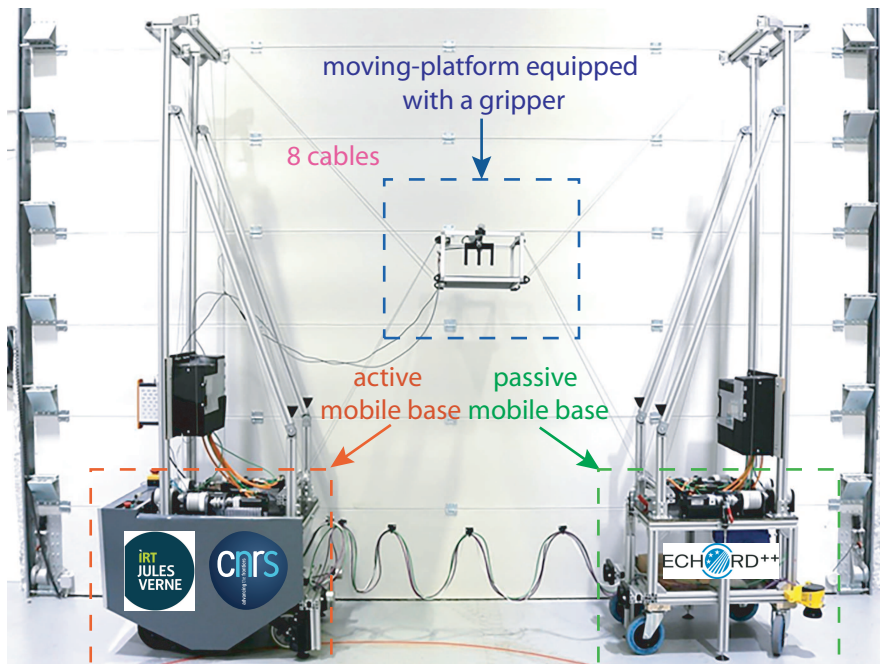Figure 2 shows the FASTKIT protoype developed in the framework of ECHORD++ FASTKIT project. It is composed of a Moving-Platform (MP) equipped with a gripper, an active Mobile Base (MB) and a passive MB connnected to each other through eight cables.

FASTKIT is capable of autonomously navigating in its environment to reach the task location referred to as a navigation mode. During this mode, the two Mobile

(a) navigation mode

(b) undeployed configuration at the task location

Active Mobile Base   Passive Mobile Base

(c) deployed configuration at the task location

Fig. 3 FASTKIT working modes

Bases (MBs) are coupled together and act as a single working unit while the MP is fixed on the two MBs (see Fig. 3(a)). The twist of the MP and the passive mobile base is equal to the twist generated by the active mobile base. No cable motion is generated during the navigation mode. The second working mode, referred to as the task mode, deploys the system at the desired location such that the desired pick or/and place operation is achievable within the defined workspace. During this mode, the passive mobile base is static while the motion of the cables and the active mobile base is used to deploy the complete system (see Figs. 3(b) and 3(c))[1]. It should be noted that during the task mode, FASTKIT is kinematically redundant due to the additional mobility of the active mobile base as explained in [12].

2.1 Main Components

The main components of FASTKIT are: (*i*) the main structure, (*ii*) the actuation system, (*iii*) its twelve pulleys, (*iv*) its MP equipped with a gripper, (*v*) Two s300 sick laser scanners, and (*vi*) two electrical cabinets. Here are the FASTKIT specifications:

- a desired workspace of 5 meters long by 2 meters high,
- a linear velocity of the moving-platform equal to 1 m/s,
- a 7 kg payload.

The 2.4 m high main structure is made up of aluminum profile bars. The eight feet of the two structures are directly fixed on the top of the two mobile bases.

2.1.1 Actuation and Transmission System

The actuation system consists of eight identical modules, each module being composed a motor, a gearbox, an elastic coupling, a transmission shaft, two bearings and a winch, as shown in Fig. fig:FASTKITactsystem.

Based on the foregoing specifications, the required maximum cable tension and maximum cable velocity are equal to 45 N and 2 m/s, respectively. As a result, 8LVA23 B&R motors coupled with 8GP30 B&R gearboxes were selected. Table 1 gives the characteristics of the selected motors.

2.1.2 Pulleys

The pulleys have been realized in such a way that the friction is a minimum and the pulley to be sustainable. Hence, the pulley must be designed such that the cable can easily roll around the sheave and that the sheave itself can rotate freely around its

---

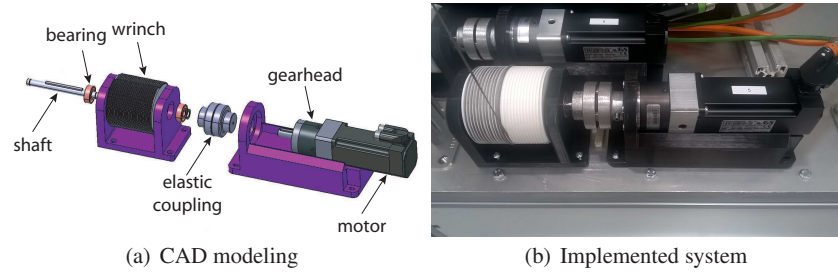[1] Videos on FASTKIT YouTube channel: `https://www.youtube.com/channel/UCJ8QRs818MBc8YSbn-bZVjA`

(a) CAD modeling   (b) Implemented system

Fig. 4 FASTKIT actuation and transmission system

Requirements	
Maximum cable tension	45 N
Maximum cable velocity	2 m/s
Actuators	
Actuation system efficiency	70%
Gearhead ratio	5:1
Wrinches	
Drum diameter	0.08 m
Motors (working point)	
Torque	0.6 Nm
Angular velocity	1600 rpm

Table 1 Characteristics of the selected motors

vertical axis. Accordingly, the sheave is equipped with a ball bearing whereas two angular contact ball bearings are used to free the sheave rotation around the vertical axis.
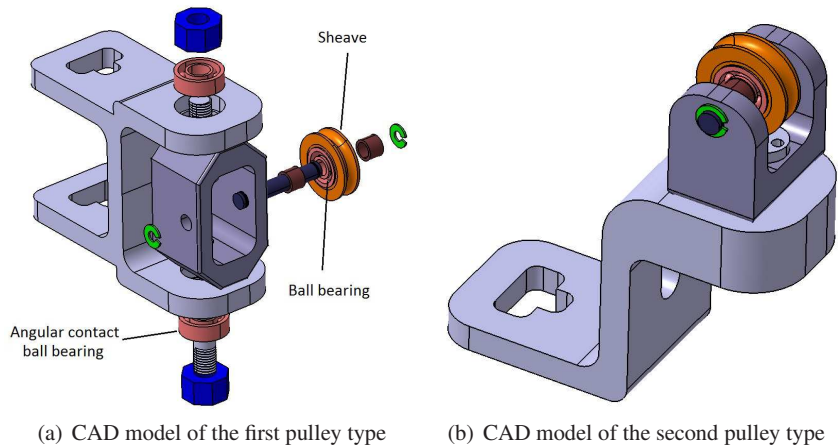

(a) CAD model of the first pulley type   (b) CAD model of the second pulley type
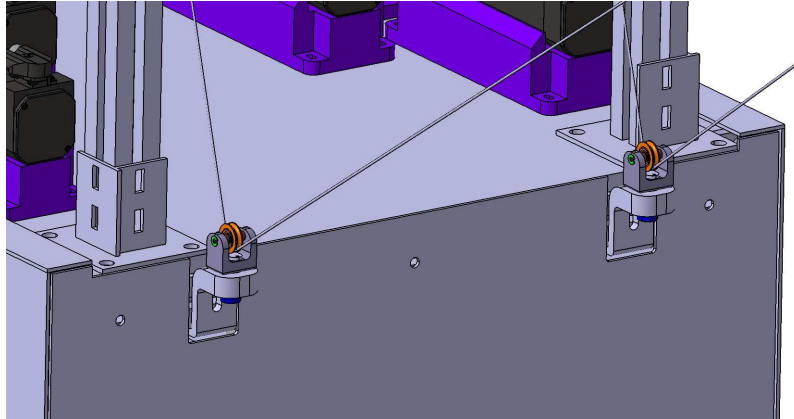
Fig. 5 FASTKIT pulleys

Fig. 6 Location of the additional pulleys for the CDPR to be in a fully constrained configuration

Figure 5(a) shows the CAD model of the eight pulleys used for the assembly of the CDPR in a suspended configuration. Figure 5(b) shows the CAD model of the additional four pulleys that have been realized to assemble the CDPR in a fully constrained configuration represented in Fig. 6.

2.1.3 Moving-Platform and Gripper

(a) CAD modeling   (b) Final assembly
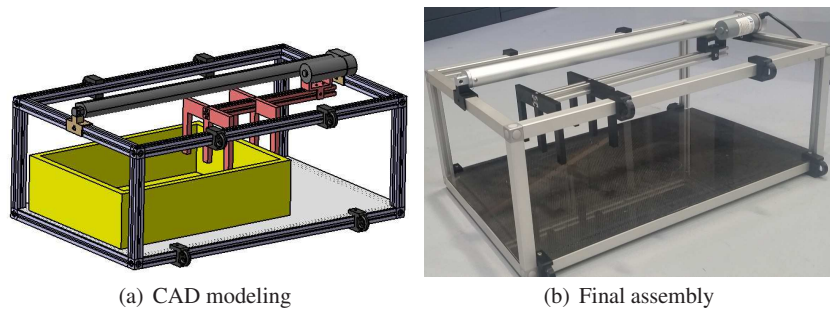
Fig. 7 Moving-platform with its gripper grabbing a storage unit box

The moving-platform has been designed to be capable of grasping, carrying and dropping a box of size 0.4 m × 0.3 m × 0.15 m, which is a typical size of the storage units used in logistics. Inner dimensions of the platform are 0.6 m × 0.36 m ×0.2 m. Figure 7(a) depicts the CAD model of the MP equipped with its gripper. Here, the mass of the moving-platform should be a minimum. The actual moving-platform,

shown in Fig. 7, weighs 5 Kg. A Firgelli linear motor [2] was used to realized the MP gripper. It should be noted that the MP tilt, required to grab and release boxes, is controlled through the cable lengths. Indeed, no exteroceptive sensor is used to manage the pick-and-place task and the MP tilt. Note that the good FASTKIT's repeatability allows us to execute this task in open-loop. On the other hand, ongoing work is dedicated to increase FASTKIT's accuracy in the initial MP positioning by means of cameras.

2.1.4 Sick Laser Scanners

Each mobile base is equipped with a s300 sick laser scanner shown in Fig. 4. It has 3 m field range and $270°$ scanning angle. This kind of scanner is usually used for obstacle avoidance and the navigation of the overall system described in Sec. 2.3.

2.1.5 Electrical Cabinets

The actuation system of the CDPR is controlled and powered by means of two electrical cabinets, one installed onto each mobile base. Those two cabinets are slightly different. Both electrical cabinets are composed of: (*i*) two variable speed drives; (*ii*) two 80V power supplies for the synchronous motors; (*iii*) one 24V power supply for the drives and (*iv*) one safety relay. In addition, the electrical cabinet embedded in the active mobile base is equipped with an industrial PC that controls the whole robot. Figure 8 shows the main electrical cabinet with the industrial PC. For the sake of compatibility, the speed drives, the power supplies and the industrial PC have been provided by the motor supplier, namely, B&R Automation ™ .

2.2 Control Strategy

The first control law that has been tested on the FASTKIT CDPR is a velocity control law. In order to implement it, the geometric and kinematic models of the CDPR are required. The velocity control is quite easy to implement and apply, but one major inconvenient arises: the cable tensions are not necessarily well distributed. Hence, during the task execution and because of ineluctable model errors, cables might get slack or too stretched. In order to cope with this undesired behavior, a torque control can be applied. First, one needs to estimate the intrinsic frictions (static, Coulomb and viscous frictions) for each motor. Once these values are established, they can be compensated in the final control law. Secondly, the optimal cable tension distribution should be computed to properly move the robot in its workspace. Several approaches to this problem are described in the literature [13, 14, 15].
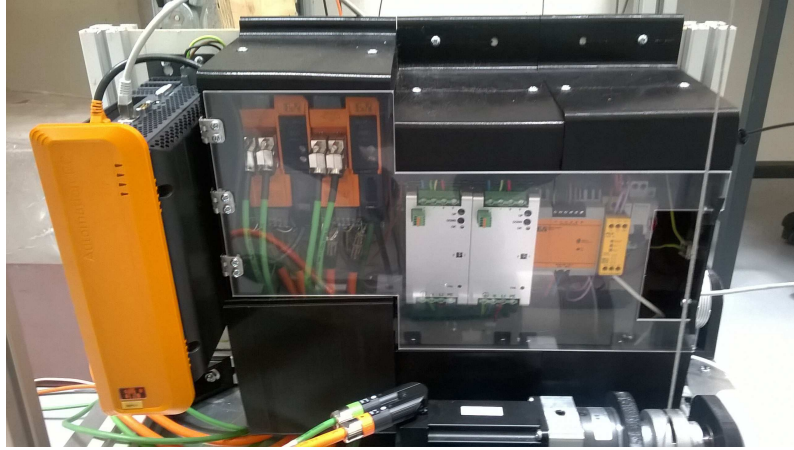
---

[2]   `https://www.firgelliauto.com/products/mini-track-actuator\`
`#ptab-specifications`

Fig. 8 The FASTKIT electrical cabinet mounted onto the active mobile base
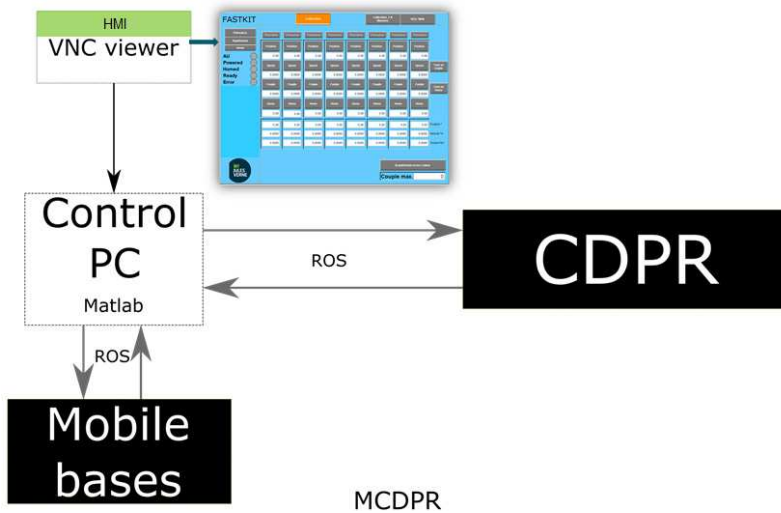

Fig. 9 The FASTKIT control architecture

The last strategy adopted in the scope of FASTKIT is described in Fig. 9. It aims to write the control algorithms in Matlab and then to communicate with the industrial PC through R.O.S. (Robot Operating System) [3]. A ROS package for communicating with the B&R™ motors had already been implemented in [11]. There is no need of code generator for Automation Studio. However, it should be noted that R.O.S. cannot run as fast as the B&R™ industrial PC. Hence, some data might get lost during the communication and the system does no longer conform to an industrial standards in terms of robustness and response time.

---

[3] http://www.ros.org/

2.3 Navigation

This section deals with the implementation of a navigation stack by means a set of interconnected algorithms. As shown in Fig. 10, those algorithms create altogether a complex decision making process:

Base driver: low-level software to control the velocity of the mobile platform ;

Sensor driver: low-level software to get sensor information, here a scanner distance readings from the two lasers;

Localization: software to localize the robot in the environment;

Collision avoidance: software, with high priority, to compute free-path for the robot w.r.t. environement dynamics ;

Path planning: global planner to compute shortest path to goal ;

User Interface: visualization tool to control robot behaviour.

Therefore, the robot is able to model its environment, plan and move to a specific goal while avoiding obstacles.

The system uses ROS navigation algorithms. The core of the framework is to provide a set of standards, namely, sensors information, actuators control and transmission protocols, to allow users to share work and generic algorithms for multiple and various robotic systems. The reader is referred to as [16] for further details about the ROS framework[4].
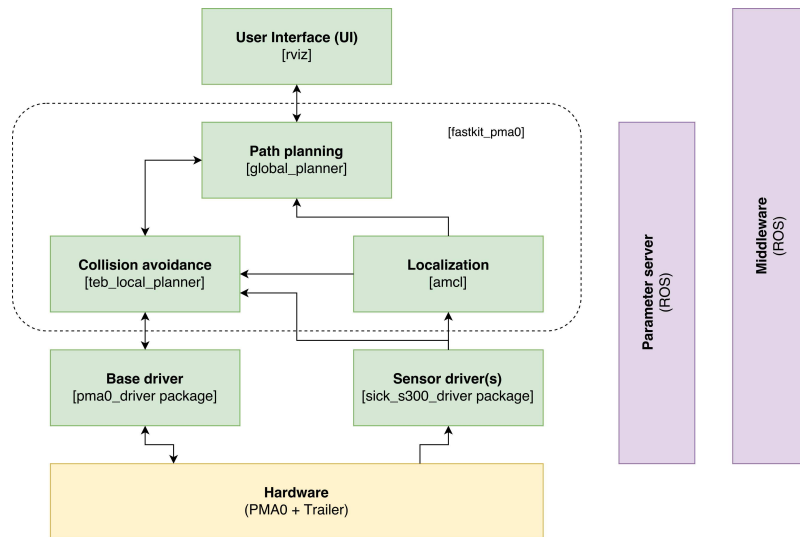

Fig. 10 Architecture of the Fastkit navigation stack. Green boxes represents software packages, names of packages are in brackets

---

[4] Ros navigation stack [online]. `http://wiki.ros.org/navigation`. Accessed: 2015-06-11.

The key challenge for an autonomous mobile robot relies on the *perception* of its environment and the *decision* it makes accordingly. By means, from the robot point of view answer to the main questions: Where am I? Where am I going? How should I get there? Navigation can therefore be separated in three problematics: (*i*) mapping, (*ii*) localization and (*iii*) planning motion. For more details about autonomous navigation, the reader is referred to as [17, 18, 19, 20, 21].
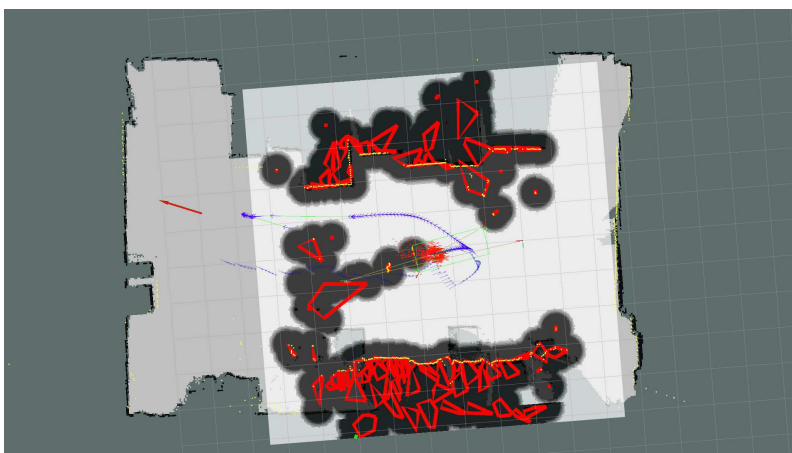

Fig. 11 Visualization of the planned trajectory towards a goal. The robot is represented by the green box. The planned trajectory is represented by the blue arrow, red polygons represent obstacles and red arrow shows the position objective. Black area represent the inflation around obstacles for the cost function that guarantees collision avoidance

Figure 11 shows a result of planned trajectory in dynamic environment. The computed polygons can be seen in red. Note that if no polygon can be found, a single point still considers the obstacle. In this scenario, people were around the mobile base, hence the planned trajectory to go toward the red arrow (i.e. objective) required a step backward and a move toward the goal while avoiding obstacles. The obtained results are very promising. However, the computation cost remains high and requires fine tuning of parameters.

3 Kinematics

The kinematic performance of any robotic system can be analyzed from its first order kinematic model [22] and the Available Twist Set (ATS). The ATS of CDPRs was defined in [23]. Thus, this section aims at presenting the kinematic model and ATS of FASTKIT. The mobile bases of FASTKIT are four-wheeled planar robots with two-DoF translational motions and one-DoF rotational motion, thus, they can
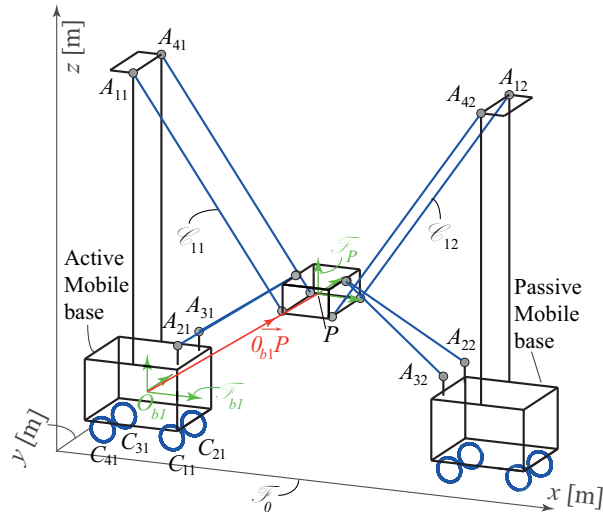
(a) FASTKIT Parameterization
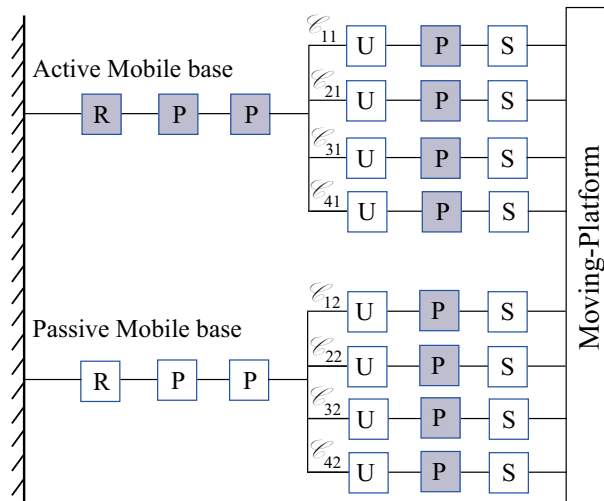
(b) Kinematic diagram of FASTKIT: active and passive joints are highlighted in gray and white, respectively

Fig. 12 FASTKIT kinematics

be modeled as a virtual RPP kinematic chain between the base frame $\mathscr{F}_0$ and the frame $\mathscr{F}_{b1}$ ($\mathscr{F}_{b2}$, resp.) attached to active (passive, resp.) mobile base.

The cables attached to the active mobile base are named in ascending order as $\mathscr{C}_{11}$, $\mathscr{C}_{21}$, $\mathscr{C}_{31}$ and $\mathscr{C}_{41}$ respectively. Similarly, the cables connected to the passive mobile base are named in ascending order as $\mathscr{C}_{12}$, $\mathscr{C}_{22}$, $\mathscr{C}_{33}$ and $\mathscr{C}_{44}$ respectively. The twist $^0\mathbf{t}_P^{cables}$ of the moving-platform as a function of cable velocities is expressed as follows:

$$\mathbf{A} \, ^0\mathbf{t}_P^{cables} = \dot{\mathbf{l}}, \tag{1}$$

where $\mathbf{A}$ is the (8×6) parallel Jacobian matrix, containing the actuation wrenches applied by the cables onto the moving-platform. The twist $^0\mathbf{t}_P = [\boldsymbol{\omega}, \dot{\mathbf{p}}]^T$ is composed of the platform angular velocity vector $\boldsymbol{\omega} = [\omega_x, \omega_y, \omega_z]^T$ and linear velocity vector $\dot{\mathbf{p}} = [\dot{p}_x, \dot{p}_y, \dot{p}_z]^T$, expressed in $\mathscr{F}_0$. $^0\mathbf{t}_P^{cables}$ denotes the platform twist only due to the cable motions. $\dot{\mathbf{l}}$ is a eight-dimensional cable velocity vector. Here, Eq. (1) can be expressed as:

$$\begin{bmatrix} \mathbf{A}_1 \\ \mathbf{A}_2 \end{bmatrix} \, ^0\mathbf{t}_P^{cables} = \begin{bmatrix} \dot{\mathbf{l}}_1 \\ \dot{\mathbf{l}}_2 \end{bmatrix}, \tag{2}$$

where $\dot{\mathbf{l}}_1 = [\dot{l}_{11}, \dot{l}_{21}, \dot{l}_{31}, \dot{l}_{41}]^T$ and $\dot{\mathbf{l}}_1 = [\dot{l}_{12}, \dot{l}_{22}, \dot{l}_{32}, \dot{l}_{42}]^T$. $\mathbf{A}_1$ and $\mathbf{A}_2$ are expressed as:

$$\mathbf{A}_1 = \begin{bmatrix} [(^0\mathbf{b}_{11} - ^0\mathbf{p}) \times \mathbf{u}_{11}]^T \ \mathbf{u}_{11}^T \\ [(^0\mathbf{b}_{21} - ^0\mathbf{p}) \times \mathbf{u}_{21}]^T \ \mathbf{u}_{21}^T \\ [(^0\mathbf{b}_{31} - ^0\mathbf{p}) \times \mathbf{u}_{31}]^T \ \mathbf{u}_{31}^T \\ [(^0\mathbf{b}_{41} - ^0\mathbf{p}) \times \mathbf{u}_{41}]^T \ \mathbf{u}_{41}^T \end{bmatrix}, \ \mathbf{A}_2 = \begin{bmatrix} [(^0\mathbf{b}_{12} - ^0\mathbf{p}) \times \mathbf{u}_{12}]^T \ \mathbf{u}_{12}^T \\ [(^0\mathbf{b}_{22} - ^0\mathbf{p}) \times \mathbf{u}_{22}]^T \ \mathbf{u}_{22}^T \\ [(^0\mathbf{b}_{32} - ^0\mathbf{p}) \times \mathbf{u}_{32}]^T \ \mathbf{u}_{32}^T \\ [(^0\mathbf{b}_{42} - ^0\mathbf{p}) \times \mathbf{u}_{42}]^T \ \mathbf{u}_{42}^T \end{bmatrix} \tag{3}$$

where $\mathbf{A}_1$ and $\mathbf{A}_2$ contain the actuation wrenches associated with cables connected to the active and passive mobile bases, respectively. $\dot{l}_{11}$ to $\dot{l}_{42}$ denote the velocity of cables $\mathscr{C}_{11}$ to $\mathscr{C}_{42}$. $^0\mathbf{b}_{11}$ to $^0\mathbf{b}_{42}$ denote the Cartesian coordinate vectors of anchor points B_{11} to B_{42} in $\mathscr{F}_0$. $^0\mathbf{u}_{11}$ to $^0\mathbf{u}_{42}$ denote the unit vector alongs cable $\mathscr{C}_{11}$ to $\mathscr{C}_{42}$. $^0\mathbf{p}$ is the Cartesian coordinate vector of the geometric center of the moving-platform expressed in frame $\mathscr{F}_0$.

3.1 First Order Kinematic Model of FASTKIT

The twist $^0\mathbf{t}_P^j$ of the moving-platform due to the cables and the mobile bases is expressed as [24]:

$$\begin{bmatrix} \mathbf{A}_1 \\ \mathbf{A}_2 \end{bmatrix} \, \mathbf{t}_P = \begin{bmatrix} \mathbf{A}_1 \, ^{b1}\mathbf{A}d_P \, \mathbf{J}_{b1} & \mathbf{0} \\ \mathbf{0} & \mathbf{A}_2 \, ^{b2}\mathbf{A}d_P \, \mathbf{J}_{b2} \end{bmatrix} \begin{bmatrix} \dot{\mathbf{q}}_{b1} \\ \dot{\mathbf{q}}_{b2} \end{bmatrix} + \begin{bmatrix} \dot{\mathbf{l}}_1 \\ \dot{\mathbf{l}}_2 \end{bmatrix}, \tag{4}$$

where $^{b1}\mathbf{A}d_P$ ($^{b2}\mathbf{A}d_P$, resp.) is called the adjoint matrix, which represents the transformation matrix between twists expressed in $\mathscr{F}_{b1}$ ($\mathscr{F}_{b2}$, resp.) and twist expressed in $\mathscr{F}_P$,

$$^{b1}\mathbf{A}d_P = \begin{bmatrix} \mathbf{I}_3 & \mathbf{0}_3 \\ -^{b1}\hat{\mathbf{r}}_P & \mathbf{I}_3 \end{bmatrix}, \quad ^{b2}\mathbf{A}d_P = \begin{bmatrix} \mathbf{I}_3 & \mathbf{0}_3 \\ -^{b2}\hat{\mathbf{r}}_P & \mathbf{I}_3 \end{bmatrix} \tag{5}$$

$^{b1}\hat{\mathbf{r}}_P$ ($^{b2}\hat{\mathbf{r}}_P$, resp.) is the cross-product matrix of vector $\overrightarrow{O_{b1}P}$ ($\overrightarrow{O_{b2}P}$, resp.) expressed in $\mathscr{F}_0$ shown in Fig. 12(a). From Eq. (4), $\dot{\mathbf{q}}_{b1}$ ($\dot{\mathbf{q}}_{b2}$, resp.) is the three-dimensional joint velocity vector of the virtual RPP kinematic chain for the active (passive, resp.) mobile base, expressed as:

$$\dot{\mathbf{q}}_{b1} = \begin{bmatrix} \dot{\theta}_1 \\ \dot{\rho}_{11} \\ \dot{\rho}_{21} \end{bmatrix}, \quad \dot{\mathbf{q}}_{b2} = \begin{bmatrix} \dot{\theta}_2 \\ \dot{\rho}_{12} \\ \dot{\rho}_{22} \end{bmatrix} \tag{6}$$

$\mathbf{J}_{b1}$ ($\mathbf{J}_{b2}$, resp.) is the (6×3) serial Jacobian matrix of the active (passive, resp.) mobile base, namely,

$$\mathbf{J}_{b1} = \begin{bmatrix} \mathbf{k}_0 & \mathbf{0}_3 & \mathbf{0}_3 \\ \mathbf{k}_0 \times {}^0\mathbf{p} & {}^0\mathbf{R}_{b1}\mathbf{i}_0 & {}^0\mathbf{R}_{b1}\mathbf{j}_0 \end{bmatrix}, \quad \mathbf{J}_{b2} = \begin{bmatrix} \mathbf{k}_0 & \mathbf{0}_3 & \mathbf{0}_3 \\ \mathbf{k}_0 \times {}^0\mathbf{p} & {}^0\mathbf{R}_{b2}\mathbf{i}_0 & {}^0\mathbf{R}_{b2}\mathbf{j}_0 \end{bmatrix} \tag{7}$$

where $\mathbf{i}_0$, $\mathbf{j}_0$ and $\mathbf{k}_0$ denote the unit vector along x_0, y_0 and z_0 axes, respectively. ${}^0\mathbf{R}_{b1}$ (${}^0\mathbf{R}_{b2}$, resp.) is the rotation matrix between frame $\mathscr{F}_0$ and frames $\mathscr{F}_{b1}$ ($\mathscr{F}_{b2}$, resp.). Equation (4) can be expressed in a matrix form as:

$$\mathbf{A}\mathbf{t}_P = \mathbf{B}_b\dot{\mathbf{q}}_b + \dot{\mathbf{l}} \tag{8}$$

$$\mathbf{A}\mathbf{t}_P = \mathbf{B}\dot{\mathbf{q}} \tag{9}$$

where $\mathbf{B} = [\mathbf{B}_b \ \mathbf{I}_m]$ is a (8×14) matrix while $\dot{\mathbf{q}} = [\dot{\mathbf{q}}_b \ \dot{\mathbf{l}}]^T$ is a fourteen-dimensional vector containing all joint velocities. As a result, Eq. (9) represents the first order kinematic model of FASTKIT.

3.2 FASTKIT Available Twist Set

The Available Twist Set (ATS) is used to characterize the twist capabilities of the moving-platform. The ATS of FASTKIT is obtained from its joint velocity limits and first order kinematic model. The joint velocity limits of the active mobile base are the following:

$$-0.2 \text{ rad.s}^{-1} \leq \dot{\theta}_1 \leq 0.2 \text{ rad.s}^{-1} \tag{10}$$

$$-0.2 \text{ m.s}^{-1} \leq \dot{\rho}_{11} \leq 0.2 \text{ m.s}^{-1} \tag{11}$$

$$-0.2 \text{ m.s}^{-1} \leq \dot{\rho}_{21} \leq 0.2 \text{ m.s}^{-1} \tag{12}$$

Once FASTKIT is deployed, its passive trailer is stabilized and does not move. Therefore, its linear and angular velocities are null, i.e.,

$$\dot{\theta}_2 = 0 \text{ rad.s}^{-1} \tag{13}$$

$$\dot{\rho}_{12} = 0 \text{ m.s}^{-1} \tag{14}$$

$$\dot{\rho}_{22} = 0 \text{ m.s}^{-1} \tag{15}$$

From Tab. 1, the cable velocity limits are the following:

$$-2 \text{ m.s}^{-1} \leq \dot{l}_{11}, \dot{l}_{21}, \dot{l}_{31}, \dot{l}_{41}, \dot{l}_{12}, \dot{l}_{22}, \dot{l}_{32}, \dot{l}_{42} \leq 2 \text{ m.s}^{-1} \tag{16}$$
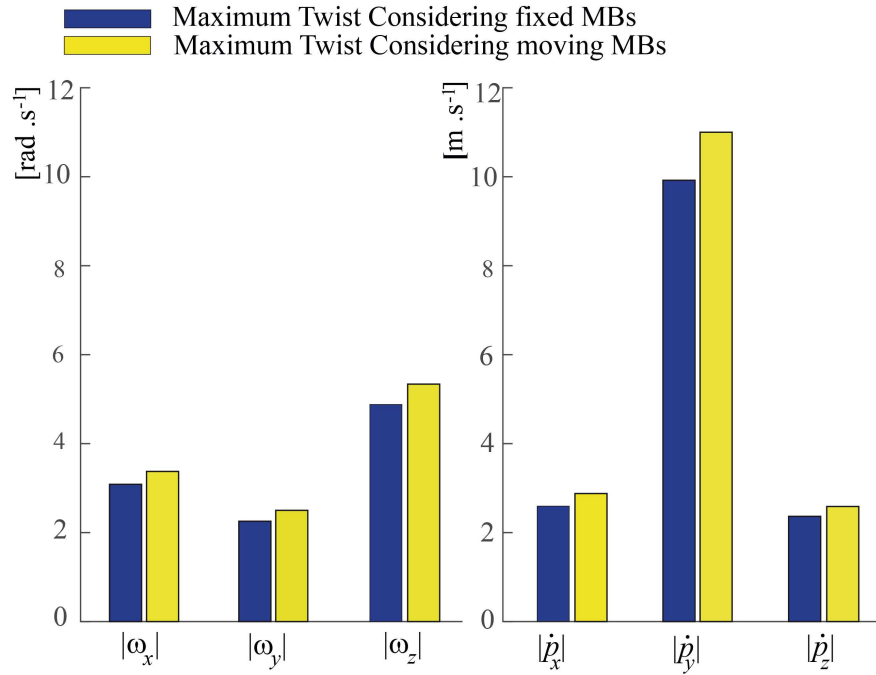
Fig. 13 Kinematic performance of FASTKIT

From the ATS of FASTKIT in the configuration shown in Fig.12(a), the maximum angular (linear, resp.) velocities of the MP about (along, resp.) *x*, *y* and *z* axes are shown in Fig. 13. It is noteworthy that the twist capacity of the moving-platform is higher when the MBs are moving than when the MBs are fixed.

4 Wrench Feasibility

The classical techniques used to analyze the workspace of CDPRs are wrench-closure workspace (WCW) [25, 26] and wrench-feasible workspace (WFW) [27,

28]. To analyze the workspace of FASTKIT, WFW has been choosen as it is more relevant from a practical viewpoint. WFW is defined as the set of platform poses for which the required set of wrenches can be balanced with wrenches generated by the cables, while maintaining the cable tension within the defined limits [27]. For a given pose, the set of wrenches a mechanism can generate is defined as available wrench set (AWS), denoted as $\mathscr{A}$.

The AWS for CDPRs only takes into account the Static Equilibrium (SE) of the moving-platform. In contrast, for FASTKIT to be in SE, both mobile bases and the moving-platform should be in SE [31]. Its a necessary and a sufficient condition for the FASTKIT to be in SE. Thus this section aims at presenting the AWS of FASTKIT by taking into account the SE of both the moving platform and the mobile bases.

4.1 Static Equilibrium of the Moving-Platform

The Static Equilibrium (SE) of the moving platform is expressed as [29, 30]:

$$\mathbf{W}\mathbf{t} + \mathbf{w}_e = \mathbf{0}, \tag{17}$$

where $\mathbf{W}$ is a (6×8) wrench matrix mapping the cable tension vector $\mathbf{t} \in \mathbb{R}^8$ onto the wrench applied by the cables on the end-effector expressed as:

$$\mathbf{W} = \begin{bmatrix} \mathbf{u}_{11} & \mathbf{u}_{21} & \mathbf{u}_{31} & \mathbf{u}_{41} & \mathbf{u}_{12} & \mathbf{u}_{22} & \mathbf{u}_{32} & \mathbf{u}_{42} \\ \mathbf{r}_{11} \times \mathbf{u}_{11} & \mathbf{r}_{21} \times \mathbf{u}_{21} & \mathbf{r}_{31} \times \mathbf{u}_{31} & \mathbf{r}_{41} \times \mathbf{u}_{41} & \mathbf{r}_{12} \times \mathbf{u}_{12} & \mathbf{r}_{22} \times \mathbf{u}_{22} & \mathbf{r}_{32} \times \mathbf{u}_{32} & \mathbf{r}_{42} \times \mathbf{u}_{42} \end{bmatrix} \tag{18}$$

$\mathbf{r}_{11}$ to $\mathbf{r}_{42}$ are the vectors pointing from the reference point P of the moving platform to the cable anchor points B_{11} to B_{42}. $\mathbf{w}_e$ denotes the external wrench applied to the end effector expressed as:

$$\mathbf{w}_e = \begin{bmatrix} \mathbf{f}_e \\ \mathbf{m}_e \end{bmatrix} \tag{19}$$

where $\mathbf{f}_e = [f_e^x, \ f_e^y, \ f_e^z]^T$ and $\mathbf{m}_e = [m_e^x, \ m_e^y, \ m_e^z]^T$ respectively denote the external forces and moment applied by the MP. The cable tension vector is bounded between a minimum tension vector $\underline{\mathbf{t}}$ and a maximum tension vector $\overline{\mathbf{t}}$,

$$\underline{\mathbf{t}} \ \leq \ \mathbf{t} \ \leq \ \overline{\mathbf{t}}. \tag{20}$$

4.2 Static Equilibrium of the Mobile Bases

The SE of both the mobile bases is defined by the moment generated at the boundaries of the mobile base footprint formed by their respective wheels, referred to as the tipping constraints. For the active mobile base, the footprint is formed by joining

the contact points of the wheels with the ground C_{11} to C_{41} in ascending order of the wheels numbering (See Fig. 12a). Similarly, the footprint of the passive mobile base is formed by joining the contact points C_{12} to C_{42} in ascending order.

Let $\mathscr{L}_{C_{11}}$ denote the boundary of the footprint between the two consecutive contact points of the wheels C_{11} and C_{21}. Let $\mathbf{u}_{C_{11}}$ be the unit vector along $\mathscr{L}_{C_{11}}$. For the active mobile base to be in SE, the moment $m_{C_{11}}$ generated about $\mathscr{L}_{C_{11}}$ should be always lower than zero, namely,

$$
\begin{aligned}
m_{C_{11}} = {} & \mathbf{u}_{C_{11}}^T((\mathbf{g}_1 - \mathbf{c}_{11}) \times \mathbf{w}_{g1}) \;+\; \mathbf{u}_{C_{11}}^T((\mathbf{c}_{11} - \mathbf{b}_{11}) \times \mathbf{t}_{11}) + \mathbf{u}_{C_{11}}^T((\mathbf{c}_{11} - \mathbf{b}_{21}) \times \mathbf{t}_{21}) \\
& + \mathbf{u}_{C_{11}}^T((\mathbf{c}_{11} - \mathbf{b}_{31}) \times \mathbf{t}_{31}) + \mathbf{u}_{C_{11}}^T((\mathbf{c}_{11} - \mathbf{b}_{41}) \times \mathbf{t}_{41}) \leq 0,
\end{aligned}
\tag{21}
$$

where $\mathbf{c}_{11}$ and $\mathbf{g}_1$ denote the Cartesian coordinate vectors of contact point C_{11} and the center of gravity G_1, respectively. $\mathbf{w}_{g1}$ denotes the weight vector of the active mobile base. Similarly for the active mobile base to be in SE, the moment generated about each boundary of the footprint must be negative. Therefore, the tipping conditions of the active mobile base are expressed as follows:

$$
\begin{bmatrix} m_{C_{11}} \\[2pt] m_{C_{21}} \\[2pt] m_{C_{31}} \\[2pt] m_{C_{41}} \end{bmatrix} =
\begin{bmatrix}
\mathbf{u}_{C_{11}}^T((\mathbf{g}_1 - \mathbf{c}_{11}) \times \mathbf{w}_{g1}) + \mathbf{u}_{C_{11}}^T((\mathbf{c}_{11} - \mathbf{b}_{11}) \times \mathbf{t}_{11}) + \mathbf{u}_{C_{11}}^T((\mathbf{c}_{11} - \mathbf{b}_{21}) \times \mathbf{t}_{21}) \\
\quad + \mathbf{u}_{C_{11}}^T((\mathbf{c}_{11} - \mathbf{b}_{31}) \times \mathbf{t}_{31}) + \mathbf{u}_{C_{11}}^T((\mathbf{c}_{11} - \mathbf{b}_{41}) \times \mathbf{t}_{41}) \\
\mathbf{u}_{C_{21}}^T((\mathbf{g}_1 - \mathbf{c}_{21}) \times \mathbf{w}_{g1}) + \mathbf{u}_{C_{21}}^T((\mathbf{c}_{21} - \mathbf{b}_{11}) \times \mathbf{t}_{11}) + \mathbf{u}_{C_{21}}^T((\mathbf{c}_{21} - \mathbf{b}_{21}) \times \mathbf{t}_{21}) \\
\quad + \mathbf{u}_{C_{21}}^T((\mathbf{c}_{21} - \mathbf{b}_{31}) \times \mathbf{t}_{31}) + \mathbf{u}_{C_{21}}^T((\mathbf{c}_{21} - \mathbf{b}_{41}) \times \mathbf{t}_{41}) \\
\mathbf{u}_{C_{31}}^T((\mathbf{g}_1 - \mathbf{c}_{31}) \times \mathbf{w}_{g1}) + \mathbf{u}_{C_{31}}^T((\mathbf{c}_{31} - \mathbf{b}_{11}) \times \mathbf{t}_{11}) + \mathbf{u}_{C_{31}}^T((\mathbf{c}_{31} - \mathbf{b}_{21}) \times \mathbf{t}_{21}) \\
\quad + \mathbf{u}_{C_{31}}^T((\mathbf{c}_{31} - \mathbf{b}_{31}) \times \mathbf{t}_{31}) + \mathbf{u}_{C_{31}}^T((\mathbf{c}_{31} - \mathbf{b}_{41}) \times \mathbf{t}_{41}) \\
\mathbf{u}_{C_{41}}^T((\mathbf{g}_1 - \mathbf{c}_{41}) \times \mathbf{w}_{g1}) + \mathbf{u}_{C_{41}}^T((\mathbf{c}_{41} - \mathbf{b}_{11}) \times \mathbf{t}_{11}) + \mathbf{u}_{C_{41}}^T((\mathbf{c}_{41} - \mathbf{b}_{21}) \times \mathbf{t}_{21}) \\
\quad + \mathbf{u}_{C_{41}}^T((\mathbf{c}_{41} - \mathbf{b}_{31}) \times \mathbf{t}_{31}) + \mathbf{u}_{C_{41}}^T((\mathbf{c}_{41} - \mathbf{b}_{41}) \times \mathbf{t}_{41})
\end{bmatrix}
\leq \mathbf{0}_4,
\tag{22}
$$

where $\mathbf{u}_{C_{21}}$, $\mathbf{u}_{C_{31}}$, and $\mathbf{u}_{C_{41}}$ are the unit vectors along the lines $\mathscr{L}_{C_{21}}$, $\mathscr{L}_{C_{31}}$ and $\mathscr{L}_{C_{41}}$, respectively. Similarly, for the passive mobile base to be in SE, the tipping conditions takes the form:

$$
\begin{bmatrix} m_{C_{12}} \\[2pt] m_{C_{22}} \\[2pt] m_{C_{32}} \\[2pt] m_{C_{42}} \end{bmatrix} =
\begin{bmatrix}
\mathbf{u}_{C_{12}}^T((\mathbf{g}_2 - \mathbf{c}_{12}) \times \mathbf{w}_{g1}) + \mathbf{u}_{C_{12}}^T((\mathbf{c}_{12} - \mathbf{b}_{12}) \times \mathbf{t}_{12}) + \mathbf{u}_{C_{12}}^T((\mathbf{c}_{12} - \mathbf{b}_{22}) \times \mathbf{t}_{22}) \\
\quad + \mathbf{u}_{C_{12}}^T((\mathbf{c}_{12} - \mathbf{b}_{32}) \times \mathbf{t}_{32}) + \mathbf{u}_{C_{12}}^T((\mathbf{c}_{12} - \mathbf{b}_{42}) \times \mathbf{t}_{42}) \\
\mathbf{u}_{C_{22}}^T((\mathbf{g}_2 - \mathbf{c}_{22}) \times \mathbf{w}_{g1}) + \mathbf{u}_{C_{22}}^T((\mathbf{c}_{22} - \mathbf{b}_{12}) \times \mathbf{t}_{12}) + \mathbf{u}_{C_{22}}^T((\mathbf{c}_{22} - \mathbf{b}_{22}) \times \mathbf{t}_{22}) \\
\quad + \mathbf{u}_{C_{22}}^T((\mathbf{c}_{22} - \mathbf{b}_{32}) \times \mathbf{t}_{32}) + \mathbf{u}_{C_{22}}^T((\mathbf{c}_{22} - \mathbf{b}_{42}) \times \mathbf{t}_{42}) \\
\mathbf{u}_{C_{32}}^T((\mathbf{g}_2 - \mathbf{c}_{32}) \times \mathbf{w}_{g1}) + \mathbf{u}_{C_{32}}^T((\mathbf{c}_{32} - \mathbf{b}_{12}) \times \mathbf{t}_{12}) + \mathbf{u}_{C_{32}}^T((\mathbf{c}_{32} - \mathbf{b}_{22}) \times \mathbf{t}_{22}) \\
\quad + \mathbf{u}_{C_{32}}^T((\mathbf{c}_{32} - \mathbf{b}_{32}) \times \mathbf{t}_{32}) + \mathbf{u}_{C_{32}}^T((\mathbf{c}_{32} - \mathbf{b}_{42}) \times \mathbf{t}_{42}) \\
\mathbf{u}_{C_{42}}^T((\mathbf{g}_2 - \mathbf{c}_{42}) \times \mathbf{w}_{g1}) + \mathbf{u}_{C_{42}}^T((\mathbf{c}_{42} - \mathbf{b}_{12}) \times \mathbf{t}_{12}) + \mathbf{u}_{C_{42}}^T((\mathbf{c}_{42} - \mathbf{b}_{22}) \times \mathbf{t}_{22}) \\
\quad + \mathbf{u}_{C_{42}}^T((\mathbf{c}_{42} - \mathbf{b}_{32}) \times \mathbf{t}_{32}) + \mathbf{u}_{C_{42}}^T((\mathbf{c}_{42} - \mathbf{b}_{42}) \times \mathbf{t}_{42})
\end{bmatrix}
\leq \mathbf{0}_4,
\tag{23}
$$

where $\mathbf{u}_{C_{12}}$, $\mathbf{u}_{C_{22}}$, $\mathbf{u}_{C_{32}}$, and $\mathbf{u}_{C_{44}}$ are the unit vectors along the lines $\mathscr{L}_{C_{12}}$, $\mathscr{L}_{C_{22}}$, $\mathscr{L}_{C_{32}}$ and $\mathscr{L}_{C_{42}}$, respectively.
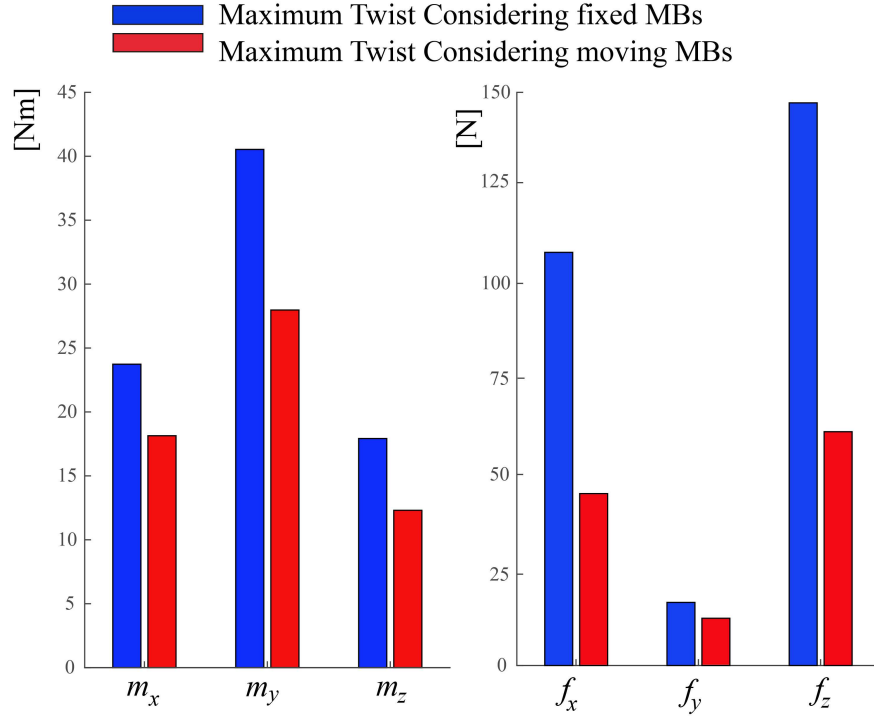

Fig. 14 Wrench capability of FASTKIT

4.3 Available Wrench Set of FASTKIT

The AWS ($\mathscr{A}$) of FASTKIT is defined by Eq. (17), respecting the cable tension limits (Eq. 20) and the tipping conditions defined by Eqs. (22) and (23). There $\mathscr{A}$ can be expressed as:

$$\mathscr{A} = \left\{ \begin{bmatrix} \mathbf{f} \\ \mathbf{m} \end{bmatrix} \in \mathbb{R}^6 \mid \begin{bmatrix} \mathbf{f} \\ \mathbf{m} \end{bmatrix} = \mathbf{W}t, \underline{\mathbf{t}} \le \mathbf{t} \le \overline{\mathbf{t}}, \ m_{C11} \le 0, \ m_{C21} \le 0, \ m_{C31} \le 0, \right.$$

$$\left. m_{C41} \le 0, \ m_{C12} \le 0, \ m_{C22} \le 0, \ m_{C32} \le 0, \ m_{C42} \le 0 \right\}. \tag{24}$$

where $\mathbf{f} = [f^x, \ f^y, \ f^z]^T$ and $\mathbf{m} = [m^x, \ m^y, \ m^z]^T$ denote the forces and moments exerted by the cables onto the moving platform, namely,

$$\mathbf{f} = -\mathbf{f}_e, \ \mathbf{m} = -\mathbf{m}_e. \tag{25}$$

From the AWS of FASTKIT in the configuration shown in Fig.12(a), the maximum absolute moments (forces, resp.) that the platform can support about (along, resp.) *x*, *y* and *z* axes are illustrated in Fig. 14. It can be noted that the wrench capability of the moving-platform is lower when the MBs are moving than when the MBs are fixed.

5 Conclusions and Future Work

This paper dealt with the design, modeling and performance analysis of a Mobile Cable-Driven Parallel Robot (MCDPR), named FASTKIT, developed in the framework of ECHORD++ FASTKIT project. FASTKIT project addressed an industrial need for fast picking and kitting operations in existing storage facilities while being easy to install, keeping existing infrastructures and covering large areas. The FASTKIT prototype consists of two mobile bases that carry the exit points of the CDPR.

FASTKIT is capable of autonomously navigating in its environment to reach the task location referred to as a navigation mode. During this mode, the two Mobile Bases (MBs) are coupled together and act as a single working unit while the MP is fixed on the two MBs. The twist of the MP and the passive mobile base is equal to the twist generated by the active mobile base. No cable motion is generated during the navigation mode. The second working mode, referred to as the task mode, deploys the system at the desired location such that the desired pick or/and place operation is achievable within the defined workspace. During this mode, the passive mobile base is static while the motion of the cables and the active mobile base is used to deploy the complete system. It should be noted that during the task mode, FASTKIT is kinematically redundant due to the additional mobility of the active mobile base as explained in [12].

The main components, the control strategy and the architecture of the navigation stack of FASTKIT were presented in this paper. Both the hardware design and the software architecture of the prototype were discussed. First, the Cable-Driven Parallel Robot (CDPR) and mobile based were studied separately. It turns out that the combination of a CDPR with two mobile bases leads to several issues such as: (*i*) the hardware + software assembly of the CDPR with the mobile bases; (*ii*) the definition of a control law to properly manage the robot motion in all its phases, and notably the deployment phase.

The main outcome of this paper is the demonstrator of a MCDPR. This demonstrator is capable of navigating in unknown environments, positioning in front of the shelves and picking some boxes on the shelf. The kinematic performance and the

wrench capability of FASTKIT have also been assessed in some specific configurations.

Therefore, a compact and reconfigurable CDPR that can work both in a fully constrained configuration and in a suspended configuration have been developed. Customized pulleys for the CDPR have designed and realized to reduce cable friction. Two electromagnetic links between the two mobile bases that rigidly connect them during the navigation phase were also implemented. From a software view point, a navigation algorithm for the mobile CDPR based on existing open-source libraries was written. A global control law that synchronizes the CDPR actuators with the active mobile base during the deployment phase was synthesized too.

There are still several open issues to be solved in the future such as: (*i*) the kinematic redundancy planning of FASTKIT and (*ii*) the wrench analysis of MCDPRs while considering both tipping and sliding conditions of their mobile bases.

References

1. Albus, J., Bostelman, R., Dagalakis, N.: The NIST spider, a robot crane. J. of Research of the Nat. Inst. of Standards and Technology 97(3), 373385 (1992)
2. Holland, C., Cannon, D.: Cable array robot for material handling (2004)
3. Bruckmann, T., Lalo, W., Sturm, C., Schramm, D., Hiller, M. (2013). Design and realization of a high rack and retrieval machine based on wire robot technology
4. Pott, A., Meyer, C., Verl, A.: Large-scale assembly of solar power plants with parallel cable robots. In: Proc. of the Int. Symp. on Robotics and 6th German Conf. on Robotics (ISR/ROBOTIK 2010), pp. 1-6. Munich, Germany (2010)
5. Kamawura, S., Kino, H., Won, C.: High-speed manipulation by using parallel wire-driven robots. Robotica 18(1), 1321 (2000)
6. Fortin-Coté, A., Cardou, P., Gosselin, C.: An admittance control scheme for haptic interfaces based on cable-driven parallel mechanisms. In: Proc. of the IEEE Int. Conf. on Robotics and Automation (ICRA 2014), pp. 819925. Hong Kong (2014)
7. P. Miermeister et al., "The CableRobot simulator large scale motion platform based on cable robot technology," 2016 IEEE/RSJ International Conference on Intelligent Robots and Systems (IROS), Daejeon, 2016, pp. 3024-3029
8. Merlet, J.P., Daney, D.: A portable, modular parallel wire crane for rescue operations. In: Proc. of the IEEE Int. Conf. on Robotics and Automation (ICRA 2010), pp. 28342839. Anchorage, AK (2010)
9. Bostelman, R., Jacoff, A., Proctor, F., Kramer, T., Wavering, A.: Cable-based reconfigurable machines for large scale manufacturing. In: Proc. of the 2000 Japan-USA Symp. on Flexible Automation. Ann Arbor, MI (2000)
10. Izard, J.B., Gouttefarde, M., Michelin, M., Tempier, O., Baradat, C.: A reconfigurable robot for cable-driven parallel robotic research and industrial scenario proofing. In: Cable-Driven Parallel Robots, Mechanisms and Machine Science, vol. 12, pp. 135148. Springer (2013)
11. Gagliardini, L., Caro, S., Gouttefarde, M., Girin, A.: Discrete reconfiguration planning for cable-driven parallel robots. Mechanism and Machine Theory 100, 313337 (2016)

12. Rasheed, T., Long, P., Marquez-Gamez, D. and Caro, S., "Optimal Kinematic Redundancy Planning For Planar Mobile Cable Driven Parallel Robots", Proceedings of the ASME 2018 International Design Engineering Technical Conferences & Computers and Information in Engineering Conference IDETC/CIE 2018, Quebec City, Canada, August 26-29, 2018.

13. Rasheed, T., Long, P., Marquez-Gamez, D. and Caro, S., 2018, "Tension Distribution Algorithm for Planar Mobile Cable-Driven Parallel Robots", In : Gosselin C., Cardou P., Bruckmann T., Pott A. (eds) Cable-Driven Parallel Robots. Mechanisms and Machine Science, vol 53, pp. 268279. Springer, Cham.

14. J. Lamaury and M. Gouttefarde. "A tension distribution method with improved computational efficiency". In Cable-driven parallel robots, pages 7185. Springer, 2013

15. L. Mikelsons, T. Bruckmann, M. Hiller, and D. Schramm. "A real-time capable force calculation algorithm for redundant tendon-based parallel manipulators". In proceedings of the 2008 IEEE International Conference on Robotics and Automation (ICRA 2008), pages 38693874.

16. Morgan Quigley, Ken Conley, Brian P. Gerkey, Josh Faust, Tully Foote, Jeremy Leibs, Rob Wheeler, and Andrew Y. Ng. Ros: an open-source robot operating system. In ICRA Workshop on Open Source Software, 2009.

17. Azim Eskandarian. Handbook of intelligent vehicles. Springer London, 2012.

18. R. Philippsen, B. Jensen, and R. Siegwart. "Autonomous navigation in dynamic environments." Springer Tracts on Advanced Robotics, 2006.

19. Michael Brady. "Robot motion: Planning and control." MIT press, 1982.

20. Howie M Choset. Principles of robot motion: theory, algorithms, and implementation. MIT press, 2005.

21. Steven M LaValle. "Planning algorithms." Cambridge university press, 2006.

22. Roberts, R. G., Graham, T., Lippitt, T., Girin, A.: On the inverse kinematics, statics, and fault tolerance of cable-suspended robots. Journal of Field Robotics, 15(10):581597, (1998)

23. Lessanibahri, S., Gouttefarde, M., Caro, S. and Cardou, P., 2018, "Twist Feasibility Analysis of Cable-Driven Parallel Robots", In : Gosselin C., Cardou P., Bruckmann T., Pott A. (eds) Cable-Driven Parallel Robots. Mechanisms and Machine Science, vol 53, pp. 128–139. Springer, Cham

24. Rasheed, T., Long, P., Gamez, D. M., and Caro, S.: Kinematic modeling and twist feasibility of mobile cable-driven parallel robots. In Advances in Robot Kinematics 2018.

25. Gouttefarde, M. and Gosselin, C.M., 2006.: Analysis of the wrench-closure workspace of planar parallel cable-driven mechanisms. *IEEE Transactions on Robotics*, 22(3), pp. 434-445.

26. D. Lau, D. Oetomo, and S. K. Halgamuge,: Wrench-Closure Workspace Generation for Cable Driven Parallel Manipulators using a Hybrid Analytical-Numerical Approach, *ASME J. Mech. Des.,* Vol. 133, 071004, 2011.

27. Gouttefarde, M., Daney, D. and Merlet, J.P., 2011. Interval-analysis-based determination of the wrench-feasible workspace of parallel cable-driven robots. *IEEE Transactions on Robotics*, 27(1), pp.1-13.

28. Cruz Ruiz, A. L., Caro, S., Cardou, P. and Guay, F., 2015, ARACHNIS : Analysis of Robots Actuated by Cables with Handy and Neat Interface Software, Cable-Driven Parallel Robots, Mechanisms and Machine Science, Volume 32, pp. 293305.

29. Kawamura, S., and Ito, K., 1993.: A new type of master robot for teleoperation using a radial wire drive system". In *Proceedings IEEE/RSJ Intelligent Robots and System (IROS)* 1993, Vol. 1, IEEE, pp. 55–60.

30. Hiller, M., Fang, S., Mielczarek, S., Verhoeven, R., and Franitza, D.: Design, analysis and realization of tendon based parallel manipulators. In *Mechanism and Machine Theory*, 40(4), pp. 429–445, 2005.

31. Rasheed, T., Long, P., Gamez, D.M., and Caro, S.: Available wrench set for planar mobile cable-driven parallel robots. In IEEE International Conference on Robotics and Automation (ICRA 2018).